Proceedings of the 2005 IEEE/ASME
International Conference on Advanced Intelligent Mechatronics
Monterey, California, USA, 24-28 July, 2005

Experimental Investigation on the Magnetic Field of a Permanent Magnet Spherical Actuator

Liang Yan, I-Ming Chen, Chee Kian Lim
School of Mechanical & Aerospace Engineering
Nanyang Technological University
Singapore 639798
pg00350830@ntu.edu.sg

Guilin Yang and Wei Lin
Mechatronics Group
Singapore Institute of Manufacturing Technology
Singapore 638075
glyang@SIMTech.a-star.edu.sg

Kok-Meng Lee
George W. Woodruff School of Mechanical Engineering
Georgia Institute of Technology
Atlanta, Georgia, USA 30332-0405
kokmeng.lee@me.gatech.edu

***Abstract*— This paper introduces the experimental study on the magnetic field of a permanent magnet (PM) spherical actuator. A new type of testbed is developed to measure the three-dimensional (3D) magnetic flux density distribution of the rotor consisting of PM poles. The captured data are nondimensionlized and normalized so that they could be referred by similar rotor designs without regard to the specific dimensions of the poles. Furthermore, the measured data are presented visually in Cartesian coordinates, which facilitates the analysis of the magnetic field generated by the rotor.**

I. INTRODUCTION

The experimental investigation of the magnetic field is one of critical topics for developing electromagnetic products. It provides a powerful tool to understand the distribution of a magnetic field which is an indispensable element to create the force/torque of these actuators. It can be used to verify the analytical or numerical result of a magnetic field as well as benefit the design optimization of products.

Experimental measurement on the magnetic flux density can be done readily in some special cases. For example, for the 1D magnetic field of electromagnets having rectangular cross-section [1] [2], the fringing flux could be ignored and the flux lines can be regarded as evenly distributed within the airgap volume. In this case, the flux density data can be taken easily at arbitrary points in the airgap by using the single-axis hall probe. Unfortunately, the rigorous requirement on the airgap in the magnetic flux loop limits the application of this measurement method. Furlani [3] simplified the flux density measurement of a PM axial-field motor by sampling the data in a characteristic point within the workspace. However, the data at this point can only reflect the variation of the magnetic field roughly. Enokizono *et al*. [4] have proposed a method to measure the flux density on a 2D plane of a single-axis motor accurately. Due to the axially symmetric structure of this motor, the magnetic field on one plane perpendicular to the axis suffices to indicate the entire magnetic field. In recent years, three-degree-of-freedom (3-DOF) electromagnetic spherical motors [5]–[10] have been developed by researchers to overcome the drawbacks of conventional spherical motion mechanisms realized by several single-axis motors connected in series or parallel. Analysis on the magnetic field of these spherical motors has been done through different means. However, so far no report has been found on the experimental work of the flux density distribution for these motors. Only FEM approach was used to simulate the variation of the flux density (radial component B_r) with respect to the spherical coordinate, ϕ or θ [10] [11]. One of the difficulties of making experiments on these 3-DOF spherical actuators might be that it is challenging to conduct the measurement of the three components of the flux density which varies in a 3D space. In this study, a testbed for the flux density measurement in a 3D space has been developed and the data have been taken within the workspace of the spherical actuator. Furthermore, the experimental result is presented visually for the easy comprehension of the magnetic field. It is worth pointing out that these data can be used to compare with the computational result from the magnetic field model as well as act as a nondimensionlized database which can be referred by other researchers.

In following sections, the working principle and the magnetic field model of the spherical actuator are reviewed. Subsequently, by using the prototype developed according to the working principle, the 3D magnetic field measurement is carried out on a testbed. Next, based on the magnetic field model, the data captured in the experiment are processed by nondimensionalization and normalization. At last, the experimental result is presented visually in a Cartesian coordinate system. And with the aid of visualization, the magnetic is analyzed.

II. MAGNETIC FIELD MODEL OF THE SPHERICAL ACTUATOR

A. Working Principle

In our previous study [12] [13], a spherical actuator that consists of a ball-shaped rotor with a full circle of PM poles and a spherical-shell-like stator with two layers of circumferential air-core coils has been proposed. The PMs of rare earth materials can generate high flux density within the actuator, and the air-core coils may simplify the torque

0-7803-9046-6/05/$20.00 ©2005 IEEE.

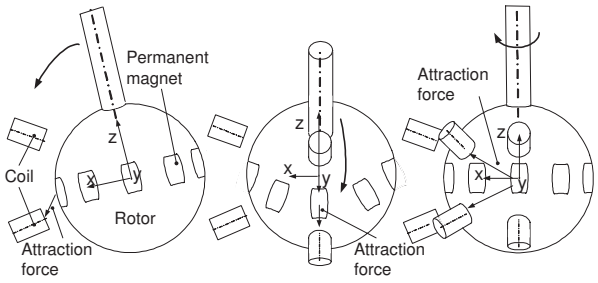

Fig. 1. 3-DOF motion of spherical actuator

model of the spherical actuator in a linear fashion. The basic working principle of the actuator is illustrated in Fig. 1. With pairs of coils in two longitudinal directions activated, the rotor creates tilting motions in two orthogonal directions as shown in Fig. 1(a) and (b). By energizing the rest of the circumferential coils, the rotor can spin about its own axis. Therefore, through varying the input currents of the coils, any desirable 3-DOF spherical motion can be generated.

B. Magnetic Field Model

Figure 2(a) illustrates the alternately magnetized PM poles along the equator of the rotor. Note that air slots exist among PM poles, which generalizes the study of poles pattern. Figure 2(b) shows the structure of a single PM pole clearly, i.e. the approximate dihedral cone enclosed by $ABCD$ and $abcd$. The dihedral cone can be defined by four parameters: α, β, R_b and R_r. On account of the material properties, the space being analyzed is divided into three regions. The air space outside the rotor is defined as Region I. The volume enclosed by $ABCD$ and $abcd$ is defined as Region II. Region III is the space enveloped by $abcdO$ where the material of soft-iron is filled in. Note that only the radial component of the flux density in Region I is able to generate a torque with respect to the rotor center. Attention is restricted on it. By using the Laplace's equation and the boundary conditions among these three regions, this radial component is formulated as [14]

$$B_{Ir}=\frac{12\mu_0 M_0 c d_4}{8\pi}\sqrt{\frac{35}{2}}r^{-6}\sin^3\theta\cos\theta(b\sin 4\phi - a\cos 4\phi), \quad (1)$$

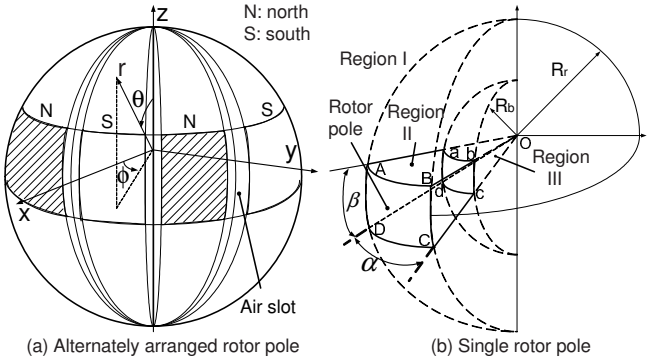

Fig. 2. Arrangement of the rotor poles

where μ_0 is the permeability of free space which has the value of $4\pi \times 10^{-7}$H/m; θ, ϕ and r form the spherical coordinates affixed on the rotor frame as shown in Fig. 2(a); M_0 is the magnitude of the residual magnetization vector $\mathbf{M}_0$ (A/m) which is related to the remanence $\mathbf{B}_{rem}$ (T) by $\mathbf{M}_0 = \mathbf{B}_{rem}/\mu_0$; and

$$d_4 = -d_4^{up}/d_4^{down}, \quad (2)$$

$$d_4^{up} = R_r^6 + \frac{9\mu_{IIrc}R_b^6R_r^9}{4(\mu_{IIIr}-\mu_{IIrc})R_b^9-(4\mu_{IIIr}+5\mu_{IIrc})R_r^9},$$

$$d_4^{down} = 5(\mu_{IIrc}-1) + \frac{9\mu_{IIrc}(4\mu_{IIIr}+5\mu_{IIrc})R_r^9}{4(\mu_{IIIr}-\mu_{IIrc})R_b^9-(4\mu_{IIIr}+5\mu_{IIrc})R_r^9},$$

R_r (mm) is the rotor radius; R_b (mm) is the radius of Region III; the dimensionless quantity, μ_{IIrc} is the relative recoil permeability of the rare-earth material in Region II; μ_{IIIr} is the relative permeability of the iron-core in Region III; a, b and c can be calculated by following integral functions

$$a+bi = \int_0^{2\pi}(-1)^{(p-1)}\cos(\phi - \frac{\alpha}{2} - \frac{\pi}{4}(p-1))e^{-im\phi}d\phi, \quad (3)$$
$$p = 1,2,3,...,8,$$

$$c = \int_0^{\pi}\sqrt{\frac{2n+1}{4\pi}\frac{(n-m)!}{(n+m)!}}P_n^m(\cos\theta)\sin^2\theta d\theta, \quad (4)$$

$P_n^m(\cos\theta)$ are associated Legendre functions [15]. To simplify the computation, only the fundamental terms, i.e. $n = 4$ and $m = \pm 4$ are considered in the derivation of the magnetic field. These integrals are only valid within the range of

$$\frac{\pi}{4}(p-1) < \phi < \frac{\pi}{4}(p-1)+\alpha, \quad p = 1,2,...8,$$
$$\frac{\pi}{2}-\frac{\beta}{2} < \theta < \frac{\pi}{2}+\frac{\beta}{2}.$$

For the rest non-magnetized regions in the rotor, the integral functions are equal to zero.

III. MEASUREMENT OF THE MAGNETIC FLUX DENSITY

In this section, a testbed is developed to measure the magnetic flux density precisely in a 3D space. Unlike previous magnetic field measurement systems, this testbed can take the three components of the flux density at any point within the workspace, and there is no special requirement on the flux lines such as even distribution. In addition, this testbed can take data either at individual points or in a specified volume automatically.

A. Prototype

Based on the working principle introduced in the preceding section, a research prototype of the 3-DOF spherical actuator [12] [13] has been developed with which the experimental measurements of the flux density can be conducted. As shown in Fig. 3, this prototype basically consists of a ball-like rotor housed within a hollow spherical stator through

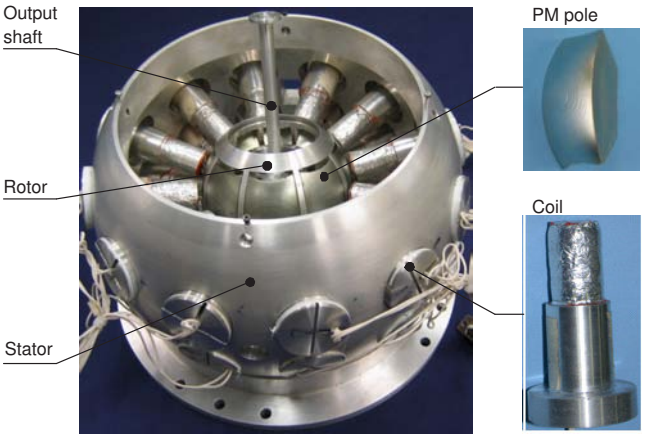

Fig. 3. Prototype of spherical actuator

a spherical bearing. The rotor has one layer of eight PM poles which are evenly distributed along its equator. On the other hand, the stator possesses twenty-four coils which are evenly grouped into two layers and symmetrically placed with respect to its equator.

B. Testbed of the Flux Density Measurement

1) Three-axis Hall Probe: In a mathematical sense, the flux density is a vector in a 3D space. In order to present the magnetic field precisely, it is necessary to measure the three components of the flux density at any measuring point surrounding the rotor. Therefore, a three-axis hall probe (Lake Shore MMZ-2502-UH) is adopted for the measurement. This aluminum stemmed probe does not affect the reading accuracy when applied to a quasi-static magnetic field such as the one created by the PM. According to the estimation, the maximum flux density of the PM poles on the rotor surface is about ±6kG which is completely covered by the maximum working range of the probe, ±30kG. Furthermore, the resolution of 0.1G and the operating temperature range from 10°C to 40°C suffice the measurement requirement in most cases.

2) Measuring Scheme: To facilitate the measurement on the magnetic field of the rotor, the measurement coordinates ϕ_p and θ_p are introduced. As illustrated in Fig. 5, the origin of the measurement coordinate (r, θ_p, ϕ_p) coincides with the rotor coordinates (r, θ, ϕ). The attitude angle θ starts from

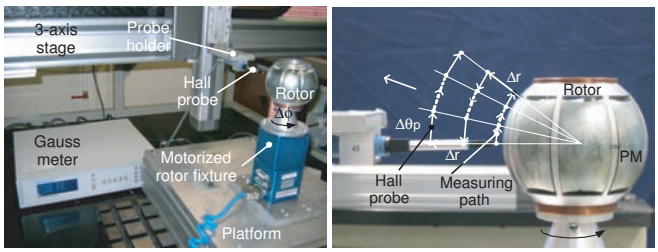

(a) Testbed (b) Measuring plane

Fig. 4. Measurement of flux density

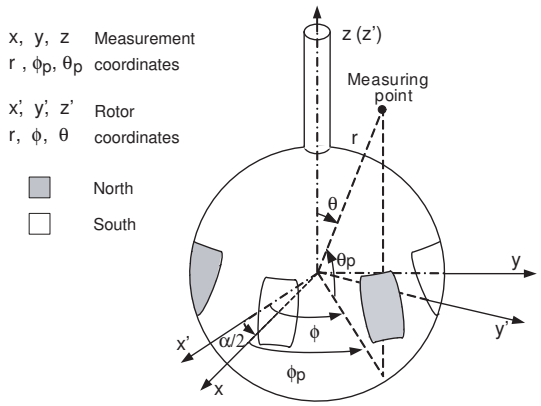

Fig. 5. Definition of θ_p and ϕ_p

the z axis whereas the angle θ_p starts from the equatorial plane; the longitude angle ϕ starts from the edge of one PM pole whereas the angle ϕ_p starts from the center of the PM pole. The relations between the two coordinate systems are $\theta = \theta_p - \pi/2$ and $\phi_p = \phi - \alpha/2$. The radial coordinates r are identical for both measurement and rotor coordinates.

Figure 4(a) shows the complete flux density measurement testbed. The Hall probe is mounted on a high precision three-axis translational motion stage so that it can pinpoint to any location near the rotor. It is also connected to the Gauss meter to display the measured flux density in three components. The Gauss meter is linked to a personal computer (PC) through a data acquisition card (DAQ). The measured flux density then can be automatically stored on the PC. The rotor is mounted on a motorized fixture that can spin along the rotor axis in 360°. Thus, it is now possible to measure the magnetic flux density in the longitudinal direction of the rotor by simply rotating the rotor using the fixture without re-orienting the Hall probe.

The Hall probe moves along a pre-determined path illustrated in Fig. 4(b) and takes measurement of flux density at sample points along the path. As the rotor structure is symmetric about the equatorial plane, the measurement is only carried out for the upper hemisphere. The measuring path starts from a point along the center axis of a PM pole and very close to the rotor surface. The measuring path is kept along a vertical plane called a *measuring plane*. The probe moves along an arc upwards on the plane while keeping at a constant normal distance d_a to the rotor surface. It can be seen from Fig. 4(b) that the neighboring sampling points keep a constant angle of $\Delta\theta_p$ with respect to the rotor center. After the probe completes an arc of $\theta_p = 30°$, the probe offsets a distance of Δr radially and then carries out measurement along the subsequent arc path. This measuring process is repeated with increasing radial distance r until the flux density is significantly small. For our measurement, the maximum motion in r-direction is 30mm. This distance far exceeds the possible location of the stator coil could be. Due to the constant angle sampling pattern, the measuring points are sparsely located when the radius r increases. It is coincident with the fact that the gradient of the flux density

decreases with the increase of r. Therefore, this sampling method is more effective than sampling with equal distance points (which requires more sampling points).

After completion of the measurement task in one measuring plane, the PC sends commands to the controller of rotor fixture to turn the rotor with an angle of $\Delta\phi_p$. The Hall probe thus "positioned" in a new measuring plane and the same data acquisition procedure is repeated.

IV. DATA PROCESSING

Thus far, the magnetic flux density measurement has been concerned. Following that, it is natural to look at the data processing so that these data could be utilized for analysis. In this section, nondimensionalization and normalization of the experimental result are discussed. The primary advantage of this data processing approach is that the resulting database can not only be applied to the magnetic field analysis of this particular spherical actuator but also act as a reference for similar designs without regard to the specific PM pole dimensions.

A. Transformation of Coordinates

As shown in Fig. 6, three components of the flux density, B_{X_h}, B_{Y_h} and B_{Z_h} are obtained based on the coordinates of the hall probe, X_h, Y_h and Z_h. In order to coincide with the spherical coordinates, r, θ and ϕ in the analytical model, it is necessary to transform these data from the Cartesian coordinates into the spherical coordinates. According to Fig. 6, following relation can be derived:

$$\begin{aligned} B_r &= B_{X_h}\cos\theta + B_{Z_h}\sin\theta, \\ B_\theta &= B_{X_h}\sin\theta - B_{Z_h}\cos\theta, \\ B_\phi &= B_{Y_h}. \end{aligned} \tag{5}$$

As mentioned before, because there is no torque generated by B_θ and B_ϕ, only the B_r is discussed following.

B. Nondimensionalization of the Experimental Result

Nondimensionalization technique is generally used in sociological, economic or mechanical areas to evaluate the weight of different inputs, such as the gap in the hydrodynamic lubrication system [16]. It offers important advantages for

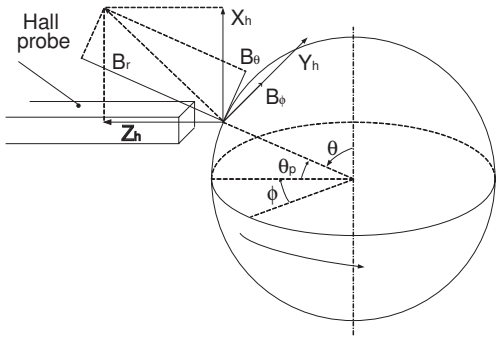

Fig. 6. Transform the flux density into the spherical coordinates

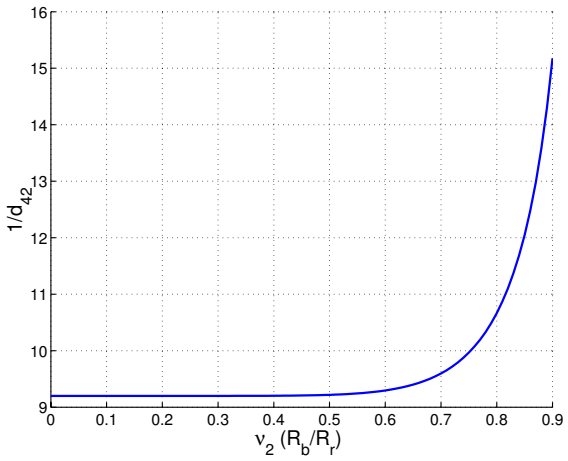

Fig. 7. Relation between ν_2 and d_{42}

the system analysis [17] [18]. (1) By using this technique, the behavior of the system can be analyzed regardless of the units used to measure the variables. One notable example is the Reynolds number that is the ratio of inertial force to the viscous force. (2) The parameters and variables are rescaled so that all computed quantities are of relatively similar magnitudes. Note that in some cases, certain quantities are vastly different sizes. This helps the model analysis by showing which variables can be thought of as "small" or "negligible" relative to others. (3) The nondimensionalization approach can also simplify the equations by reducing the number of variables. (4) In this paper, the raw data of this experiment is nondimensionalized and normalized to form a standard database. This database can be referred by other similar designs. The specific process is introduced as follows.

1) Nondimensionalization of the Radius Parameters: In order to facilitate the discussion following, Eqns. (1) and (2) are reorganized as

$$B_{Ir}=\frac{15\mu_0 M_0 c d_{4,2}}{8\pi}\sqrt{\frac{35}{2}}\nu_1^6\sin^4\theta\sqrt{a^2+b^2}\cos(4\phi+\phi_0) \tag{6}$$

where

$$d_{4,2} = -d_{4,2}^{up}/d_{4,2}^{down}, \tag{7}$$

$$d_{4,2}^{up}=1+\frac{9\mu_{IIrc}}{4(\mu_{IIIr}-\mu_{IIrc})\nu_2^3-(4\mu_{IIIr}+5\mu_{IIrc})(\frac{1}{\nu_2})^6}, \tag{8}$$

$$d_{4,2}^{down}=5(\mu_{IIrc}-1)+\frac{9\mu_{IIrc}(4\mu_{IIIr}+5\mu_{IIrc})}{4(\mu_{IIIr}-\mu_{IIrc})\nu_2^9-(4\mu_{IIIr}+5\mu_{IIrc})}, \tag{9}$$

$\nu_1 = R_r/r$, $\nu_2 = R_b/R_r$, ϕ_0 is defined by $\cos\phi_0 = a/\sqrt{a^2+b^2}$ and $\sin\phi_0 = b/\sqrt{a^2+b^2}$. Note that both ν_1 and ν_2 are nondimensionalized coefficients varying between 0 and 1. Therefore, the question of computing the flux density according to the dimensional parameters, R_b, R_r and r becomes the question of calculating the flux density from nondimensionalized parameters, ν_1 and ν_2.

2) Normalization of the Experimental Result: Here the normalization or rescaling of the experimental raw data is carried out. As a matter of convenience, denote the experimental result after the coordinate transformation in Section IV-A as B^e_{Ir}. The process of normalization is described as follows.

• **Step One:** According to Eqn. (7), the relationship between ν_2 and $1/d_{4,2}$ is illustrated in Fig. 7. It can be found out that when $0 < \nu_2 < 0.5$, $1/d_{42}$ does not vary much, always being 9.2. In physics, it means that the magnetized material at the core of the rotor does not help much to improve the flux density of the rotor. Between $0.5 < \nu_2 < 0.7$, $1/d_{4,2}$ increases slightly. After $\nu_2 = 0.7$, $1/d_{4,2}$ augments drastically, which indicates that when R_b is near to R_r or when the thickness of the PM pole is approaching a very thin size, the flux density of the rotor drops down quickly. According to this graph, the minimum value of $1/d_{4,2}$ can be chosen as the scale to normalize the experimental data. Recall the design parameter of the spherical rotor. It can be obtained that $\nu_2 = 20/46.5 < 0.5$, which leads to the minimum value of $1/d_{4,2}$. Therefore, the experimental result on the current rotor could be thought of as the standard value after the scaling of $B^e_{Ir}/\frac{1}{9.2}$ or $9.2B^e_{Ir}$.

• **Step Two:** Inspection of Eqn. (6) shows that the term $\mu_0 M_0 c$ is related to the parameters of this particular rotor design. Therefore, to generalize the database, the experimental result has to be normalized further by $B^e_{Ir}/\mu_0 M_0 c$. Note that this step is also a nondimensionalization process because all of the variables with units are scaled.

• **Step Three:** Further observation of Eqn. (6) shows that ϕ_0 is pertaining to the particular constants a and b which in turn are determined by the rotor parameter α. A normalized database should avoid this phenomena so that it is applicable to the general rotor design. As a result, the experimental data described in spherical coordinates is shifted an angle of $\phi_0/4$ in ϕ direction, denoted as $B^e_{Ir}(\phi - \phi_0/4)$.

Consider the three steps above. Eventually, the data in the standard database, B^N_{Ir}, is obtained from B^e_{Ir} by

$$B^N_{Ir} = \frac{9.2B^e_{Ir}(\phi - \phi_0/4)}{\mu_0 M_0 c}. \tag{10}$$

Note that B^N_{Ir} is completely nondimensionalized. It is a function of ν_1, ϕ and θ, all of which are dimensionless arguments.

C. Computation of the Flux Density from the Standard Database

Having known that the standard database has been established, it is natural to consider how to derive the magnetic flux density of a PM rotor that has different parameter values from the current rotor by using this standard database.

To distinguish from the current design, a generalized rotor is specified with parameters having primes, M'_0, a', b', c' and ϕ'_0, where a' and b' can be derived from α' by Eqn. (3) whereas c' can be derived from β' by Eqn. (4). From the database, the magnetic flux density of this rotor can be computed by

$$B_{Ir} = \mu_0 M'_0 c' d'_{4,2} B^N_{Ir}(\phi + \phi'_0/4), \tag{11}$$

where $d'_{4,2}$ can be obtained from R'_b and R'_r by Eqn. (7).

V. VISUALIZATION AND ANALYSIS OF THE EXPERIMENTAL RESULT

In a measurement system, after the data processing, an effective way is supposed to be found to represent the measured value in a form which can be easily recognized by the observer [19]. In this article, the measured magnetic flux density is represented visually. Based on this visualization, analysis of the magnetic field could be carried out. As a specific case but without loss of generality, the representation and the analysis in this section are based on the magnetic field of the current PM rotor design.

A. Visualization of the Magnetic Field

Visualization of the experimental results aids in understanding the flux density distribution. With reference to Fig. 5, one set of three parameters, r, θ_p and ϕ_p can specify one point in the rotor coordinates. Thus the flux density at that point can be determined. Including the flux density component B_{Ir}, there are totally four parameters. Obviously, it is difficult to present four parameters in a 3D space. To solve this problem, r is given a certain fixed value. Then by varying θ_p and ϕ_p, the values of the flux density can be obtained. In Cartesian coordinates defined by θ_p, ϕ_p and B_{Ir}, the variation of B_{Ir} forms a surface geometrically. Corresponding to different values of r, one set of surfaces can be obtained to show the flux density variation of the magnetic field visually in a 3D space.

B. Comparison with the Computational Result

With knowledge of the magnetic field model that has been derived, it is necessary to compare the computational result with the experimental result. Some comparisons are presented in Fig. 8. One of the meshed surface in the figure represents the experimental result of the flux density distribution, whereas the other stands for the computational result from the mathematical model. Basically, the computational result matches the variation of the experimental result well. Along the equator of the rotor, i.e. ϕ_p direction, eight positive/negative peaks can be observed. This phenomena is caused by the eight alternately magnetized PM poles on the rotor equator. In contrast, the flux density declines gradually in θ_p direction, which is consistent with the known fact.

However, difference can still be observed between the experimental and computational results, which varies periodically. This is caused the fact that during the computation of the magnetic field model, only the fundamental terms of the scalar potential in the form of spherical harmonic expansion (SHE) are made use of.Adding more terms may reduce the difference.

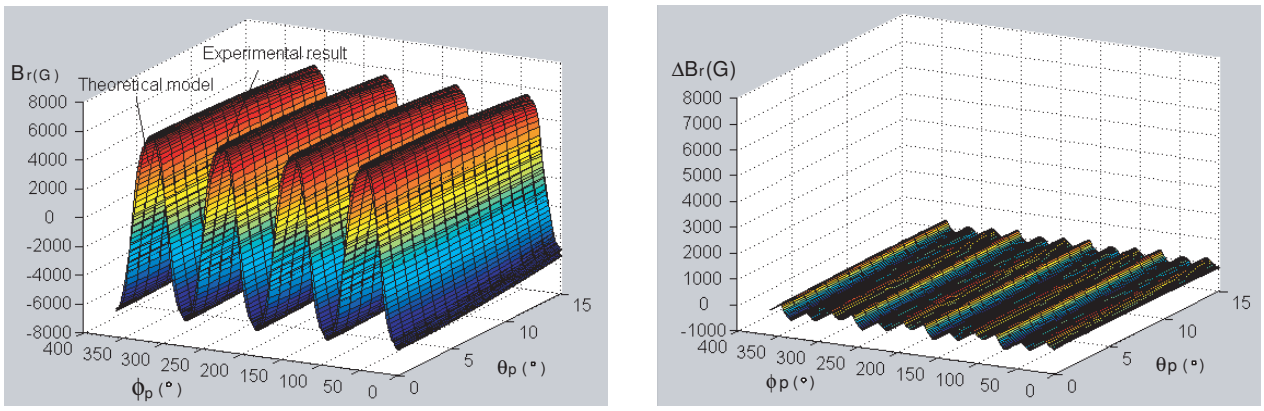

(a) Experimental vs. theoretical results

(b) Difference between experimental vs. theoretical results

Fig. 8. Comparison of experimental result and theoretical model ($d_a = 0.5$mm)

VI. CONCLUSION

The 3D magnetic field measurement testbed developed in this article contributes to the magnetic field study of the 3-DOF PM spherical actuators. As an improvement on its predecessors that can only achieve 1/2D measurement, this testbed can locate any point within the 3D workspace and take the data of flux density in terms of vectors. Another contribution of this paper is the nondimensionalization and normalization of the experimental data, which broaden the application of these data from the current rotor with particular dimensions to a parametric rotor design. In addition, after the data processing, the experimental data are presented in a 3D Cartesian coordinate system visually, which facilitates the observation and analysis of the magnetic field greatly.

ACKNOWLEDGMENT

This work is a collaborative research project among Nanyang Technological University (NTU), Singapore Institute of Manufacturing Technology (SIMTech) and Georgia Institute of Technology (Gatech) under the project grant U02-A-040B. The authors would like to acknowledge the assistance from Dr. Weihai Chen, Mr. Thng Soong Moong Thomas, and Mr. Jialin Su.

REFERENCES

[1] P. M. Mintchev, C. D. Christov, and A. M. Rahman, "Analysis of flux in electromagnets having rectangular cross-section," *IEEE Transactions on Magnetics*, vol. Mag-11, no. 5, pp. 1550–1551, September 1975.

[2] P. M. Mintchev, "Optimum design of electromagnets by means of the goodness factor approach," *IEEE Transactions on Magnetics*, vol. Mag-23, no. 5, pp. 3777–3779, September 1987.

[3] E. P. Furlani, "A method for predicting the field in permanent-magnet axial-field motors," *IEEE Transactions on Magnetics*, vol. Mag-28, no. 5, pp. 2061–2066, September 1992.

[4] M. Enokizono, M. Morikawa, S. Fujiyama, J. Sievert, and I. Serikawa, "Distribution of local magnetic properties in three-phase induction motor model core," *IEEE Transactions on Magnetics*, vol. 35, no. 5, pp. 3937–3939, September 1999.

[5] A. Foggia, E. Oliver, and F. Chappuis, "A new three degrees of freedom electromagnetic actuator," in *Proceedings of IAS*, vol. 35, New York, July 1988, pp. 137–141.

[6] B. B. Bederson, S. R. Wallace, and L. E. Schwartz, "Control and disign of the spherical pointing motor," in *IEEE International Conference on Robotics and Automation*, Atlanta, US, May 1993, pp. 630–636.

[7] R. L. Hollis, S. Salcudean, and A. P. Allan, "A six degree-of-freedom magnetically levitated variable compliance fine motion wrist," *IEEE Transactions on Robotics and Automation*, vol. 7, no. 3, pp. 320–332, June 1991.

[8] G. S. Chirikjian and D. Stein, "Kinematic design and commutation of a spherical stepper motor," *IEEE/ASME Transactions on Mechatronics*, vol. 4, no. 4, pp. 342–353, December 1999.

[9] J. Pei, "Methodology of design and analysis of variable-reluctance spherical motors," Ph.D. dissertation, Georgia Institute of Technology, GA, USA, 1990.

[10] J. Wang, G. W. Jewell, and D. Howe, "Analysis, design and control of a novel spherical permanent-magnet actuator," in *IEE Proceedings: Electric Power Applications*, vol. 145, no. 1, January 1998, pp. 61–71.

[11] ——, "Spherical actuators with multiple degrees-of-freedom," in *IEE Colloquium on Limited motion electrical actuation systems*, no. 1998/494, October 1998, pp. 8/1–8/6.

[12] C. K. Lim, L. Yan, I. M. Chen, G. L. Yang, and W. Lin, "Mechanical design & numerical electromagnetic analysis of a dc spherical actuator," in *2004 IEEE Conference on Robotics, Automation and Mechatronics*, Singapore, December 2004, pp. 536–541.

[13] L. Yan, C. K. Lim, I. M. Chen, G. L. Yang, and W. Lin, "A hybrid approach for magnetic field analysis," in *2004 IEEE Conference on Robotics, Automation and Mechatronics*, Singapore, December 2004, pp. 530–535.

[14] L. Yan, I. Chen, C. Lim, G. Yang, W. Lin, and K. M. Lee, "Torque modeling of a spherical actuator based on lorentz force law," in *2005 IEEE International Conference on Robotics and Automation*, Barcelona, Spain, April 2005, pp. 3657–3662.

[15] N. Virchenko and I. Fedotova, *Generalized Associated Legendre Functions and Their Applications*. USA: World Scientific Publication, 2001.

[16] Z. M. Zhang, Y. Y. Zhang, Y. B. Xie, Z. X. Chen, D. M. Qiu, and J. Zhu, *Theory of Hydrodynamic Lubrication of Journal Bearing*. P.R.China: China Higher Education Press, 1986.

[17] C. C. Lin and L. A. Segel, *Mathematics applied to deterministic problems in the natural sciences*. US: Macmillan Publishing Co., Inc., 1974.

[18] A. C. Fowler, *Mathematical Models in the Applied Sciences*. US: Cambridge University Press, 1997.

[19] J. P. Bentley, *Principles of Measurement Systems*. Singapore: John Wiley & Sons, Inc., 1988.